ASTM INTERNATIONAL

Materials Performance and Characterization

Robert Pilarczyk,[1] Ricardo Actis,[2] Joseph Cardinal,[3] Scott Carlson,[3] James Harter,[4] Joshua Hodges,[5] Scott Prost-Domasky,[6] and Guillaume Renaud[7]

DOI: 10.1520/MPC20190210

Successful Round Robin Analyses Resulting from the Engineered Residual Stress Implementation Working Group

Materials Performance and Characterization

doi:10.1520/MPC20190210 available online at www.astm.org

Robert Pilarczyk,[1] Ricardo Actis,[2] Joseph Cardinal,[3] Scott Carlson,[3] James Harter,[4] Joshua Hodges,[5] Scott Prost-Domasky,[6] and Guillaume Renaud[7]

Successful Round Robin Analyses Resulting from the Engineered Residual Stress Implementation Working Group

Manuscript received August 14, 2019; accepted for publication February 24, 2020; published online August 11, 2020.

[1] Hill Engineering, LLC, 3083 Gold Canal Dr., Rancho Cordova, CA 95670, USA (Corresponding author), e-mail: rtpilarczyk@hill-engineering.com, https://orcid.org/0000-0002-9691-1305

[2] Engineering Software Research and Development, Inc., 111 West Port Plaza, Suite 825, St. Louis, MO 63146, USA

[3] Southwest Research Institute, 6220 Culebra Rd., San Antonio, TX 78238, USA

[4] LexTech Inc, 1452 Yankee Park Pl., Dayton, OH 45458, USA

[5] Hill Engineering, LLC, 3083 Gold Canal Dr., Rancho Cordova, CA 95670, USA

[6] Analytical Processes/Engineered Solutions, Inc., 6669 Fyler Ave., St. Louis, MO 63139, USA

[7] National Research Council Canada, Building M-14, 1200 Montreal Rd., Ottawa, Ontario K1A 0R6, Canada

Reference

R. Pilarczyk, R. Actis, J. Cardinal, S. Carlson, J. Harter, J. Hodges, S. Prost-Domasky, and G. Renaud, "Successful Round Robin Analyses Resulting from the Engineered Residual Stress Implementation Working Group," *Materials Performance and Characterization* https://doi.org/10.1520/MPC20190210

ABSTRACT

The application of engineered residual stresses (ERSs) on aircraft structure provides an opportunity to significantly extend the total fatigue life of critical components. In order to reach required service life goals within budgetary constraints, the ability to implement ERS into analyses is essential. However, it has been repeatedly demonstrated that in order to properly quantify, apply, and analyze ERSs, sophisticated analytical tools, advanced technical knowledge, and specialized training are required. The ERS implementation (ERSI) working group provides the opportunity for collaborative development of best practices for government, contractors, and engineers supporting the implementation of ERSs into life predictions. The ultimate goal of the working group is to develop a more holistic framework for the implementation of ERS, with validated tools and processes for application to aircraft structures, minimizing expensive test programs, and offering benefits to all stakeholders. The ERSI Fatigue Crack Growth Analysis Method committee has taken the initiative to develop round robin fatigue life predictions for cold expanded holes. An initial round robin effort was completed to quantify the epistemic uncertainties in the prediction of fatigue crack growth, given a fixed set of input data. The results of this round robin are presented, including the variations in the predictions and comparison with test results, as well as lessons learned and best practices.

Keywords

fatigue, residual stress, round robin, fracture, cold expanded holes, damage tolerance

Introduction

The engineered residual stress implementation (ERSI) working group is an organization initially established by individuals within and supporting the United States Air Force (USAF) to (1) develop a roadmap for the implementation of engineered deep residual stress for fatigue and fracture critical aerospace components, (2) highlight the gaps in the state-of-the-art, and (3) define the most effective ways to document requirements and guidelines for a more holistic, physics-informed method for fleet-wide implementation. Since its inception in 2016, ERSI has grown to over 120 participants from different countries, Department of Defense organizations, national labs, universities, original equipment manufacturers (OEMs), industry partners, and USAF Aircraft Structural Integrity Program managers.

ERSI is structured into eight committees, each with a particular focus on key aspects of the implementation of ERS into fatigue crack growth (FCG) predictions. The FCG Analysis Methods committee is chartered with identifying best practice and analysis approaches for the implementation of ERS. One key initiative of the committee was the development and execution of an FCG analysis round robin, providing an opportunity to evaluate aspects of the analysis process, identifying current gaps, and developing best practices.

An initial FCG Analysis Methods round robin was completed to quantify the epistemic uncertainties in the prediction of crack growth life, given a fixed set of input data. Specific input data were developed to minimize the effect of random uncertainties; however, the analysts were free to use any means to incorporate the residual stresses into their FCG life prediction. The effort was an opportunity to exercise various analytical methods, comparing them to experimental results and uncovering strengths and weaknesses of the various approaches.

TEST METHOD AND OVERVIEW

Four conditions, including baseline non–cold expansion (Cx) and Cx, were selected for the round robin effort. For all Cx conditions the FTI split sleeve cold expansion (SSCx) process was used. These conditions were selected based on the relevance to actual aircraft conditions as well as clear documentation of all the inputs provided to the analysts. Additional details of the experimental results were previously published and included the coupon geometry, maximum stress, stress ratio (R), fatigue lives, crack shapes defined by markerbanding, and other specific details associated with the experimental programs.[1–4] Specific inputs were provided to participants, including coupon geometries, material properties, initial crack (size, shape, location, and orientation), the constant amplitude loading spectrum, boundary conditions, and residual stress (developed via the contour method).[5] FCG rate data (da/dN versus ΔK) were supplied in tabular form. All holes were processed with the 16-0-N SSCx standard tool kit.[6] The level of applied expansion for these two conditions was calculated knowing the initial hole diameter, the mandrel maximum diameter, and the sleeve thickness. From these known dimensions, the applied expansion could be calculated with the final residual expansion determine knowing the initial and final hole diameters.

A summary of the provided inputs is included in Table 1 and figure 1, showing a graphical representation of the residual stress distribution that was provided to each participant in a tabular format. The residual stress

TABLE 1
Benchmark specimen conditions

Case #	Material	Specimen Type	Thickness, in (mm)	Width, in (mm)	Hole Diameter, in (mm)	Edge Distance, in (mm)	Applied Expansion, %	Loading	Max Stress ksi, MPa
1	2024-T351	Non-CX	0.25 (6.35)	4.00 (101.6)	0.50 (12.7)	2.0 (50.8)	N/A	Constant Amplitude ($R = 0.1$)	10 (68.9)
2		CX					3.7		25 (172.4)
3		Non-CX				0.6 (15.24)	N/A		10 (68.9)
4		CX					3.2		25 (172.4)

FIG. 1 Residual hoop stress for cases 2 and 4: center hole (bottom) and short edge distance conditions (top). The left edge and lower left corner represent the edge of the hole and the initial crack locations assumed for analysis, respectively.

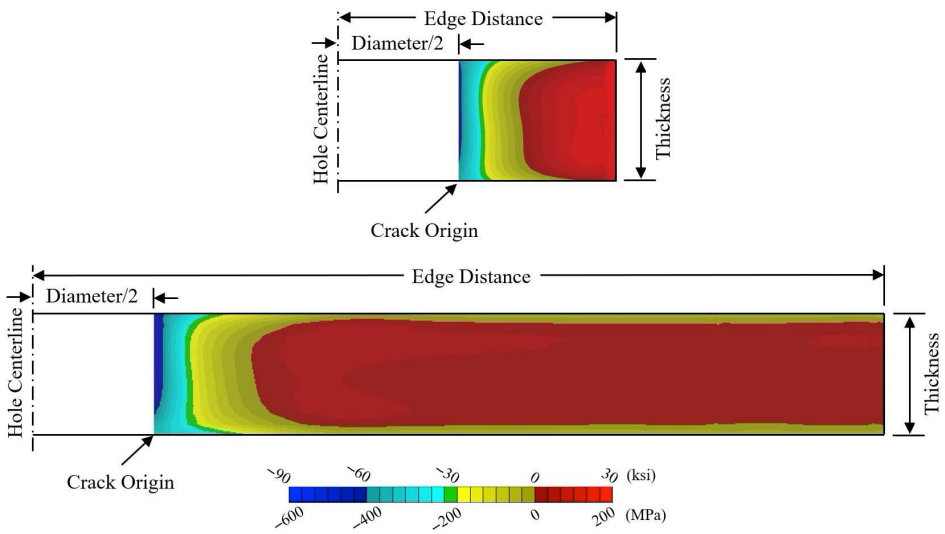

distribution shown in figure 1 was determined via the contour method and represents the hoop residual stress on the crack plane that is developed from the SSCx process.[5,7] The residual stress field would represent the component of stress acting in and out of figure 1 and is the main residual stress field effecting the crack growth performance of a component or part. Analysts were free to use any means to incorporate the provided residual stress tabular data into the crack growth prediction, any software suite, etc.; however, it was important that the analysts adhered closely to other guidance provided so that the variability in the predictions was limited to the aspects left to the analyst's discretion.

ANALYSIS APPROACH

Eight analysts participated in the round robin, each taking a different approach to analyze the conditions provided. Analysts were free to choose their preferred software, resulting in several different software packages utilized within the round robin. The classical fracture mechanics-based software programs NASGRO (Version 8.2) and AFGROW (Version 5.3.3.23) were used in addition to software packages that coupled finite element analysis (FEA) to FCG software such as Broad Application for Modeling Failure (BAMF) (Version 5.0) and the Crack Propagation Analysis Tool (CPAT) (Version 1.2). In each of these latter two approaches, the FEA software used was StressCheck (Version 10.3).

Many analysts took the round robin effort as an opportunity to evaluate multiple analytical approaches, highlighting the strengths and weaknesses of each. The NASGRO analyses used the Fawaz-Anderson corner crack solutions as well as advanced univariant (1-D) and bivariant (2-D) weight function solutions. The AFGROW analyses used the "classic Newman-Raju corner crack solutions" with a 2-D Gaussian integration method to estimate the residual K values in each crack growth direction.[8] The Newman-Raju curve fit equations were used for parametric angles of 5° and 80° along the crack front for the c and a-direction, respectively. Both NASGRO and AFGROW used conventional linear elastic fracture mechanics approaches in performing the analyses in that the computed stress intensity factors (SIFs) were linearly combined (applied stress plus residual stress) and used to compute ΔK and then da/dN. However, the NASGRO analyses used a NASGRO equation fit to the supplied tabular da/dN data, whereas the AFGROW analyses used the Harter-T interpolation method[9] on the tabular data to compute da/dN.

It was determined that the classic Newman-Raju corner cracked hole stress intensity solutions (K_I) are approximately 10–15 % lower than the Fawaz-Anderson Advanced corner crack solutions in the a-direction. This resulted in overly conservative predictions using the Classic solution in AFGROW. At the time of the round robin effort, the Gaussian integration method was not available for use in the AFGROW Advanced Model Interface. Subsequently, this capability was added to AFGROW and these predictions were repeated with much better results. The NASGRO and AFGROW approaches compute crack growth at two crack tips: the a-tip in the bore of the hole and the c-tip along the surface. This contrasts with the coupled FEA approaches that compute crack growth at multiple points along the crack front. A summary of the key modeling factors for each submission is detailed in Tables 2 and 3.

Coupled FEA-FCG Methods

Solution Domain

Coupled FEA-FCG analysis provides users flexibility in modeling actual geometries and simulate boundary conditions representing the specimen in a fatigue test fixture. CPAT utilized a solution domain that consisted of half model symmetry through the hole with constraints to simulate the effects of the grip in the testing fixture, whereas BAMF users utilized a full through hole model with constraints to mimic the grips in the testing fixtures (fig. 2).

Crack Front Shape—Basic Assumptions

The direction of crack growth is normal to the crack front, and the crack grows in the plane of the initial crack. The shape of the crack is represented by a spline curve passing through equally spaced points along the crack front. The number of points is user-defined, and the coordinates of the points are updated automatically every crack increment. The user-specified crack increment Δa, controls the largest Δa increment of crack growth between each analysis step:

$$\Delta a_{max} = (farthest\ point\ on\ crack\ front) * (max.\Delta a\ percent) \quad (1)$$

For these analyses, users utilized a max. Δa between 1–5 %. In the case of CPAT, each crack increment was computed as follows:

1. Every point i along the crack front is characterized by the load cycle ratio R_i and stress intensity factor (SIF) amplitude ΔK_i as obtained from the finite element solution.

TABLE 2
Summary of modeling considerations for baseline cases #1 and #3

	Key Modeling Factors Baseline Cases 1 and 3				
	Software		Crack Definition		
Submission Number	Lifing Software	FE Software	Crack Front Shape	Number of Crack Front Points	Stress Intensity Calculation
1	CPAT	StressCheck	Multipoint	30	Contour Integral Method
2	CPAT	StressCheck	Multipoint	20	Contour Integral Method
3	AFGROW	N/A	Elliptical	2	Standard, Classic Newman-Raju
4a	NASGRO	N/A	Elliptical/Straight Thru	2	NASGRO CC08/TC13 univariant WF
4b	NASGRO	N/A	Elliptical/Straight Thru	2	NASGRO CC16/TC03 Fawaz/Anderson
4c	NASGRO	N/A	Elliptical/Straight Thru	2	NASGRO CC10/TC13 bivariant WF
4d	NASGRO	N/A	Elliptical/Straight Thru	2	NASGRO CC08/TC13 univariant WF
4e	NASGRO	N/A	Elliptical/Straight Thru	2	NASGRO CC16/TC03 Fawaz/Anderson
4f	NASGRO	N/A	Elliptical/Straight Thru	2	NASGRO CC10/TC13 bivariant WF
5	BAMF	StressCheck	Multipoint	11	Contour Integral Method
6	AFGROW	N/A	Elliptical/Straight Thru	2	Standard, Classic Newman-Raju
7	CPAT	StressCheck	Multipoint	15	Contour Integral Method
8	AFGROW	N/A	Elliptical/Straight Thru	2	Standard, Classic Newman-Raju

TABLE 3
Summary of modeling considerations for Cx Cases #2 and #4

	Key Modeling Factors Cx Cases 2 and 4					
	Software		Crack Definition			
Submission Number	Lifing Software	FE Software	Crack Front Shape	Number of Crack Front Points	RS Incorporation Approach	Stress Intensity Calculation
1	CPAT	StressCheck	Multipoint	30	Crack Face Pressure (B-Spline)	CIM-LC
2	CPAT	StressCheck	Multipoint	20	Crack Face Pressure (Legendre Polynomial)	CIM-LC
3a	AFGROW	N/A	Elliptical	2	2-D Gaussian Integration (Free Surface)	Classic Newman-Raju
3b	AFGROW	N/A	Elliptical	2	2-D Gaussian Integration (5 degrees)	Classic Newman-Raju
3c	AFGROW	N/A	Elliptical	2	2-D Gaussian Integration (10 degrees)	Classic Newman-Raju
4g	NASGRO	N/A	Elliptical/Straight Thru	2	Bivariant WF	NASGRO CC10/TC13 Bivariant WF
4h	NASGRO	N/A	Elliptical/Straight Thru	2	Bivariant WF	NASGRO CC10/TC13 Bivariant WF
4i	NASGRO	N/A	Elliptical/Straight Thru	2	Univariant WF	NASGRO CC08/TC13 Univariant WF
4j	NASGRO	N/A	Elliptical/Straight Thru	2	Univariant WF	NASGRO CC08/TC13 Univariant WF
5	BAMF	StressCheck	Multipoint	11	Polynomial Fit Crack Face Pressure	CIM-LC
6	AFGROW	N/A	Elliptical/Straight Thru	2	1-D Gaussian Integration (20 % from free surface)	Classic Newman-Raju
7	CPAT	StressCheck	Multipoint	15	Crack Face Pressure (Legendre Polynomial)	CIM-LC
8	BAMF	StressCheck	Multipoint	10	Crack Face Pressure (Legendre Polynomial)	CIM-LC

2. The corresponding values of $(da/dN)_i$ are computed by linear interpolation from the available da/dN–ΔK data.
3. For the point with $(da/dN)_{max}$, it computes the corresponding $\Delta N = \Delta a_{max}/(da/dN)_{\max}$ (fig. 3).
4. With ΔN fixed, it uses $(da/dN)_i$ of each point for computing the corresponding increments $\Delta a_i = (da/dN)_i\ \Delta N$.

In the case of BAMF, a similar approach is used:

1. BAMF calculates the SIF that is due to mechanical load $(K_{\text{app}})_i$ and residual stress $(K_{rs})_i$ using StressCheck, and passes this information to AFGROW.
2. AFGROW computes R_i and ΔK_i for each control point along the crack front for a single cycle and then computes the corresponding $(da/dN)_i$ by interpolation; AFGROW computes the Δa_i for each cycle, until a single value $\Delta a_i/a_i$ is greater than the user input.
3. AFGROW passes new crack lengths to StressCheck, and the process is repeated.

Crack Meshing

The mesh was updated automatically for each crack increment. The mesh was refined around the crack front with two layers of elements graded in geometric progression toward the crack front for the extraction of the SIFs using

FIG. 2

Solution domain and boundary conditions for CPAT (top) and BAMF (bottom).

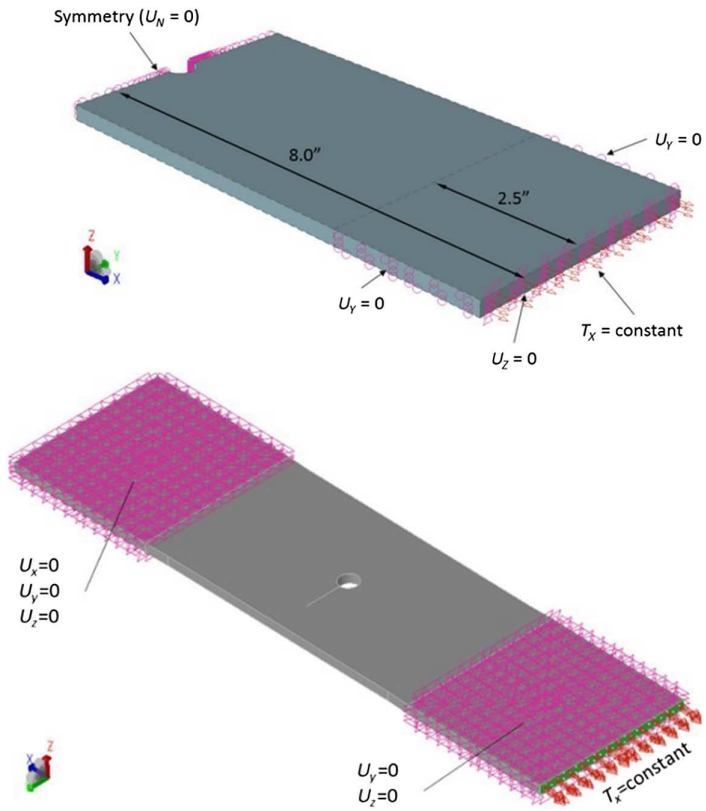

FIG. 3

Computation of Δa for each point along the crack front.

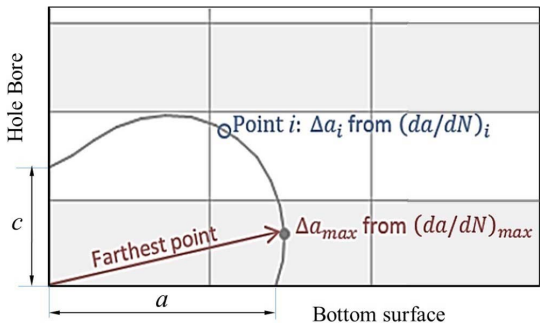

the contour integral method (CIM).[10] The solution was obtained by the finite element method, and control of the error of approximation in the computation of the SIFs was provided by increasing the number of degrees of freedom by p-extension (hierarchically increasing the order of the approximating displacement functions) on a fixed mesh.[10] A typical mesh refinement along the crack front of a corner crack is shown in figure 4.

Incorporation of Residual Stresses

The residual stress data, provided in tabular form, needed to be in equation form to be utilized as a crack face traction for both CPAT and BAMF. Each analyst utilized a different fitting algorithm to model the residual stress

FIG. 4 Typical tetrahedral element mesh refined along the crack front (highlighted in red). The detailed view shows the size of an element in the crack front relative to the size of the surface crack.

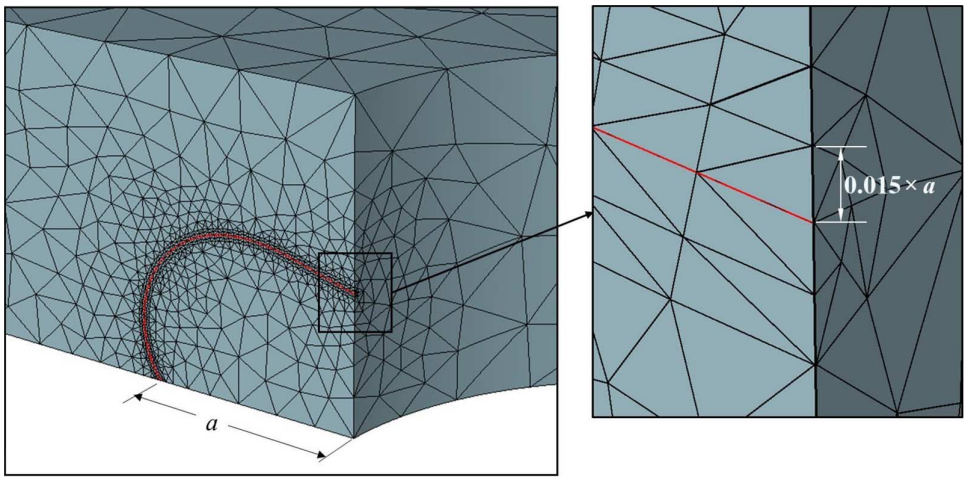

field. For example, figure 5 shows a typical interpretation of the tabular data for case #4 using Legendre polynomials of order 16 with a fitting error of 0.42 % in L2-norm.

The formula-based residual stress resulting from the fitting was applied as a normal traction to the crack face to compute SIFs as a result of residual stresses, $K_{RES,}$ at points along the crack front using the CIM for loaded cracks (CIM-LC).[11] Because the principle of superposition is used, the effect of the residual stresses and the mechanical load were treated as two separate load cases during the analysis. For each load case, the SIF is computed at each point along the crack front. For the remote traction, the K_{MECH} is computed using the CIM and for K_{RES} using the CIM-LC. For specimens without Cx holes, only the mechanical load is applied.

FIG. 5 Input RS data points (left) and fitted RS (right) data for case #4 with Legendre polynomial of order 16.

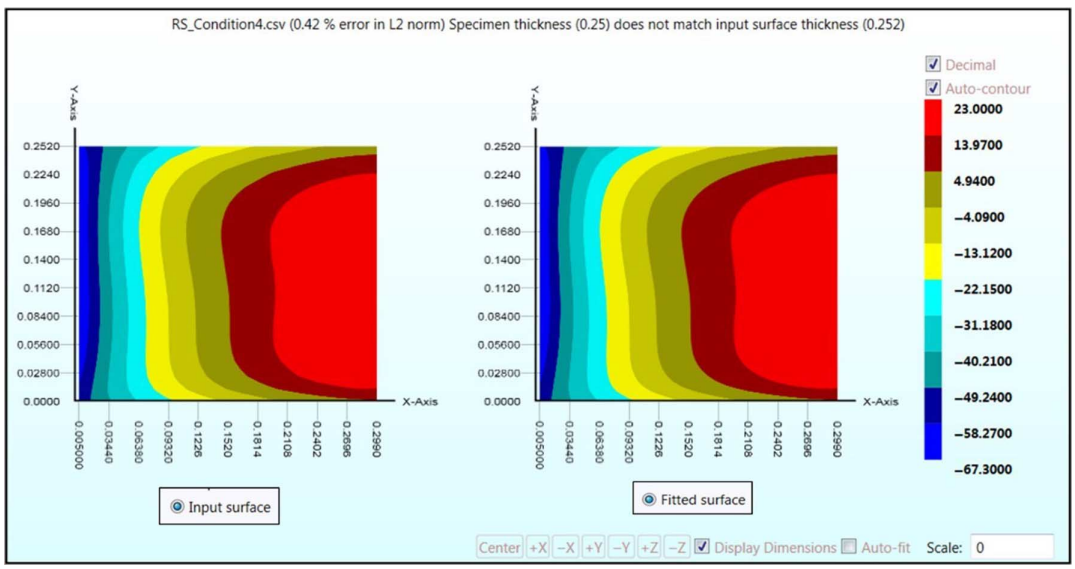

Incorporating FEA-SIFs into the Crack Growth Analysis

The method of superposition was used to incorporate the SIF in the crack propagation algorithm. The driver of fatigue crack propagation is the SIF amplitude ΔK, and the residual stresses only affect the R as shown in **figure 6**. At each point along the crack front, the values of K_{MECH} and K_{RES} are computed from the finite element solutions, next the values of $K_{\max}$, $K_{\min}$, $\Delta K = (K_{\max} - K_{\min})$ and R are computed from which da/dN is obtained by interpolation, and finally the corresponding crack increment is determined.

Life Prediction

Crack propagation rates derived from the available da/dN–ΔK data obtained at fixed load ratios were used for the predictions. Linear log-log interpolation was used for finding da/dN for load ratios not covered by the experimental data. For a given ΔK_{calc} and R_{calc} at a point along the crack front, the two bounding curves (R_a and R_b) were identified (bounding the computed values with respect to R_{calc}), and the da/dN values were interpolated along the two curves to produce $\log(da/dN_a)$ and $\log(da/dN_b)$, respectively, corresponding to ΔK_{calc}. Then, a second interpolation is performed between the curves to obtain the final da/dN.

$$\log\frac{da}{dN} = \frac{\log\frac{da}{dN_b} - \log\frac{da}{dN_a}}{R_b - R_a}(R_{calc} - R_a) + \log\frac{da}{dN_a} \tag{2}$$

Typical calculation records along a crack front are shown in **figure 7**.

No extrapolation was used. When the R value at a point along the crack front was less than $R = -0.25$, only one interpolation was performed along the "$R = -0.25$ curve" using $K_{\max}$ instead of ΔK.

FIG. 6

Superposition to incorporate the effect of residual stresses in crack propagation.

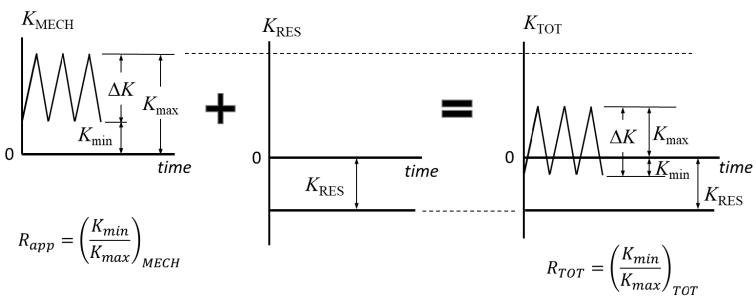

FIG. 7 Typical calculation records at points along the crack front.

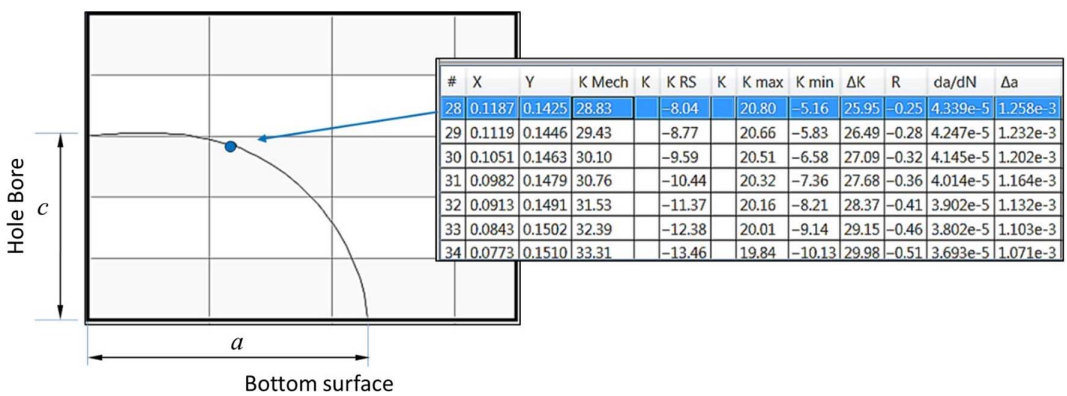

#	X	Y	K Mech	K	K RS	K	K max	K min	ΔK	R	da/dN	Δa
28	0.1187	0.1425	28.83		−8.04		20.80	−5.16	25.95	−0.25	4.339e-5	1.258e-3
29	0.1119	0.1446	29.43		−8.77		20.66	−5.83	26.49	−0.28	4.247e-5	1.232e-3
30	0.1051	0.1463	30.10		−9.59		20.51	−6.58	27.09	−0.32	4.145e-5	1.202e-3
31	0.0982	0.1479	30.76		−10.44		20.32	−7.36	27.68	−0.36	4.014e-5	1.164e-3
32	0.0913	0.1491	31.53		−11.37		20.16	−8.21	28.37	−0.41	3.902e-5	1.132e-3
33	0.0843	0.1502	32.39		−12.38		20.01	−9.14	29.15	−0.46	3.802e-5	1.103e-3
34	0.0773	0.1510	33.31		−13.46		19.84	−10.13	29.98	−0.51	3.693e-5	1.071e-3

Results

A summary of the key modeling factors for each submission is detailed in **Tables 2** and **3**. The submitted predictions were compared to experimental results looking at surface and bore crack length versus cycles (c versus N, a versus N), crack growth rates versus cycles (dc/dN versus N, da/dN versus N), crack growth rate versus crack length (dc/dN versus c, da/dN versus a), crack aspect ratio evolution (a/c versus a/t), SIF comparisons (K_{MECH} and K_{RES}), through thickness transition, critical crack lengths, and the slope at the transition point. FCG predictions (c versus N) and crack propagation rates (dc/dN versus c) for all cases are compared with the experimental results in **figures 8–11**, with classic AFGROW predictions colored green, NASGRO predictions colored blue, and coupled FEA-FCG software predictions colored red. Crack aspect ratio comparisons (a/c versus a/t) are also included in **figure 12** for cases #2 and #4. These results are of

FIG. 8 Prediction of fatigue crack propagation life (left) and propagation rates (right) for case #1. Symbols without lines correspond to experimental data.

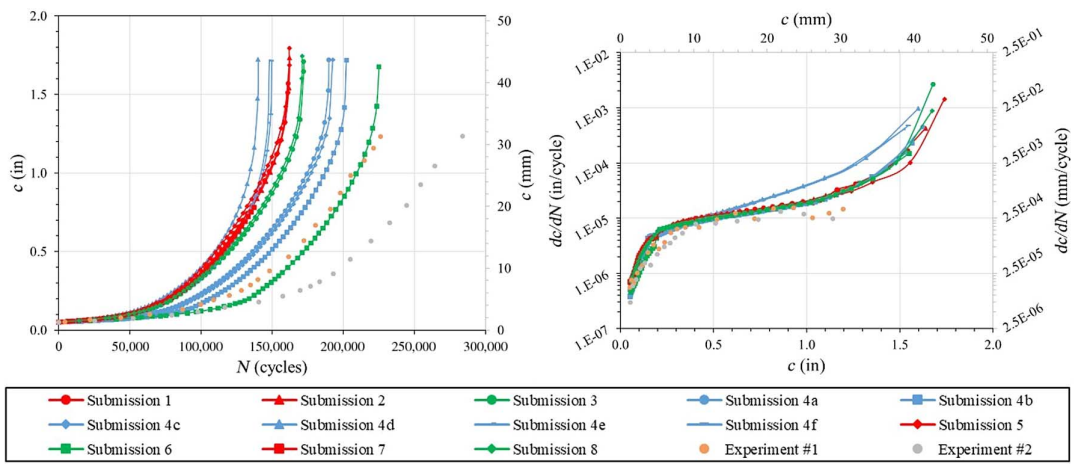

FIG. 9 Prediction of fatigue crack propagation life (left) and propagation rates (right) for case #2. Symbols without lines correspond to experimental data.

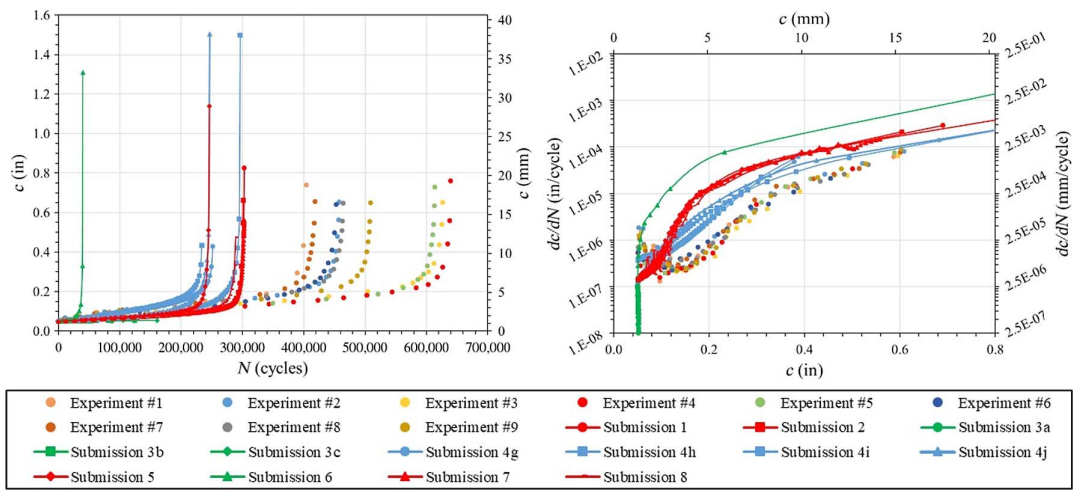

FIG. 10 Prediction of fatigue crack propagation life (left) and propagation rates (right) for case #3. Symbols without lines correspond to experimental data.

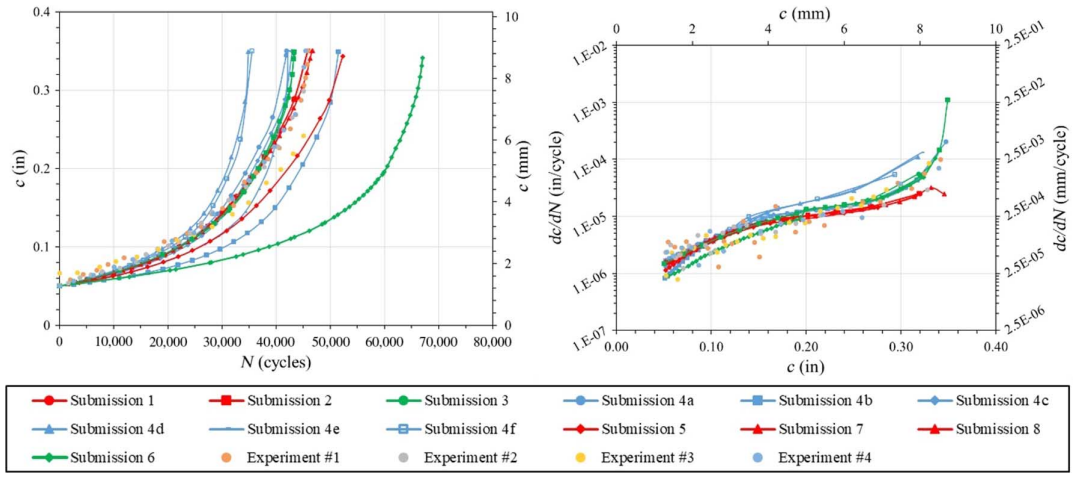

FIG. 11 Prediction of fatigue crack propagation life (left) and propagation rates (right) for case #4. Symbols without lines correspond to experimental data.

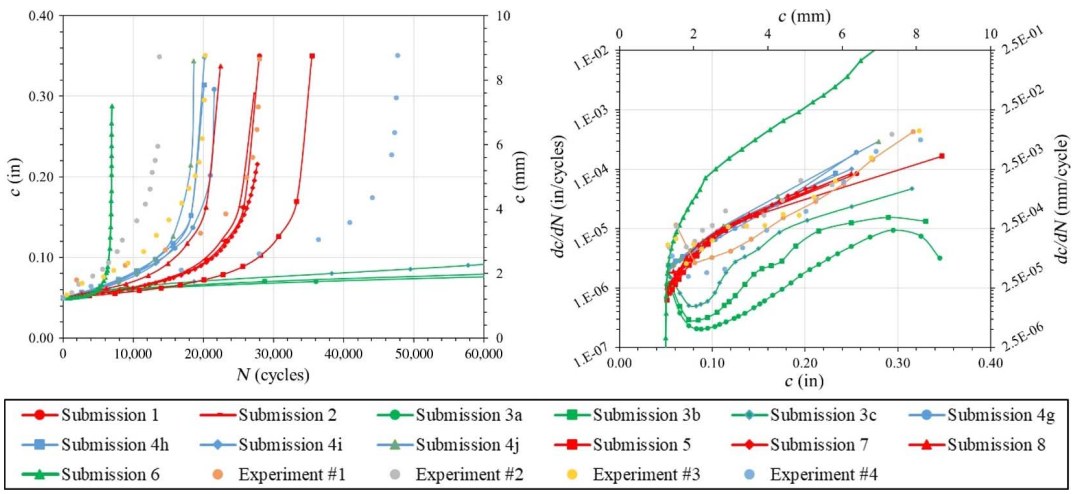

particular interest to highlight similarities and differences between the results from the various prediction approaches.

Discussion

For cases #1 (fig. 8) and #3 (fig. 10), both non-Cx holes and the life predictions were generally consistent across all the analytical approaches. For case #1, the predicted lives ranged between 40–90 % (underpredicted) of the average experimental lives, indicating some possible differences between the provided rate data and the experimental coupons. For case #3, the FCG predictions and growth rates were consistent across all the analytical approaches and correlated with observed experimental results. Crack growth rates were computed with the secant

FIG. 12 Prediction of crack aspect ratios for Cx case #2 (left) and case #4 (right). Symbols without lines correspond to experimental data.

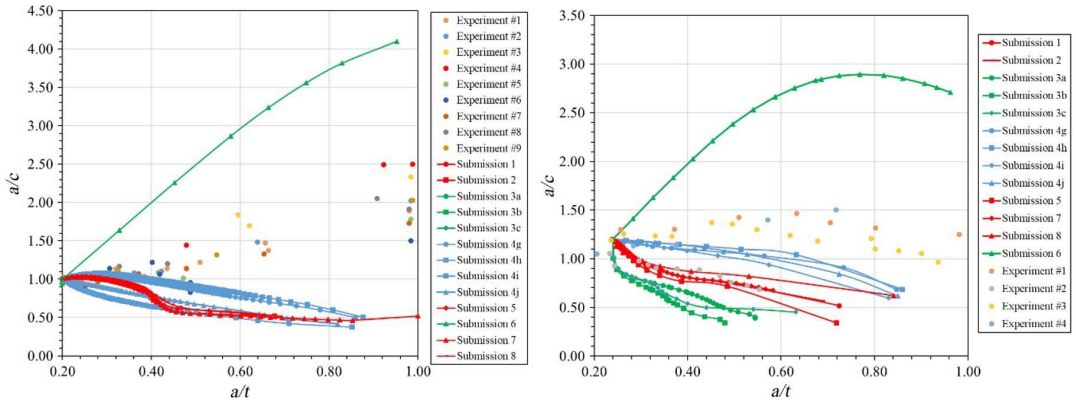

method.[12] Comparisons of the predicted to the measured growth rates versus crack length in the right side of **figure 8** and **figure 10** show reasonable agreement.

For cases #2 (**fig. 9**) and #4 (**fig. 11**), both Cx holes and the AFGROW classic Newman-Raju solutions utilizing 1-D and 2-D Gaussian integration to compute the residual SIFs were quite inconsistent with the 2-D cases overpredicting the experimental life. The NASGRO and FEA-FCG life predictions were consistent for both cases #2 and #4. Similar to the results for case #1, case #2 predicted lives ranged between 45–60 % (underpredicted) of the average experimental lives. Initial growth rates underpredicted observed experimental results followed by overpredictions for crack lengths greater than approximately 0.10-in. (2.54-mm). For case #4, predicted lives were within the range of the experimental results. Submission 6 tended to be an outlier relative to the other submissions. Several attempts to contact the submitter to review the analysis approaches and determine the root cause of the differences was unsuccessful. Ultimately, the predictions for submission 6 were included in the summary for completeness; however, additional interpretation of the root cause is not possible.

Comparisons of the predicted to the measured crack growth rates (dc/dN) in the right side of **figures 9** and **11** have mixed conclusions. In the centered hole coupons (case #1 and case #2) (symbols in **fig. 9**), measured crack growth rates are initially about 1 to 5E-5 in./cycle (2.54 to 12.7E-4 mm/cycle), then dip down, bottoming out at approximately 2E-7 in./cycle (5.08E-6 mm/cycle) at a surface crack c length of 0.15 in. (3.81 mm); then, they grow monotonically higher until failure. Predicted crack growth rates of all submissions missed the dip demonstrated from the test data. In the short edge margin holes (case #3 and case #4), the measured rates of two of the test coupons did not exhibit a dip, which is shown in the previous two cases (symbols in **fig. 11** right). Only submissions 3a, 3b, and 3c (all AFGROW with 2-D Gaussian integration) demonstrated a dip; the other 10 submissions predicted no dip. However, the crack growth rate reduction predicted by these three AFGROW solutions resulted in excessively long lives. This may be explained by the lower K-solution used in the a-direction that drove the net K-solution to fall near or below the crack growth threshold.

What is the possible cause of the inability of each submission to consistently pick up the dip in the crack growth rates? One cause could be crack shielding; in this case, crack closure (crack face closing before the applied load is fully released) and thus crack deceleration could be present, but this is unknown because none of the submissions modeled closure. Recent investigations have also indicated the interaction of the crack with the residual stress or the possibility of an initial shakedown of stresses or both, resulting in the redistribution of stress.[13,14] Another possible cause is the uncertainty in the residual stresses supplied and presumably used in each submission. It is well established that the contour method used to determine the residual stresses has higher levels of spatial uncertainty near the free surfaces.[15,16] It is possible that the residual stresses that were supplied do

not accurately represent the initial or evolving residual stress in the test coupons and thus the correct stress state was not modeled in the submissions.

Crack aspect ratio comparisons (see **fig. 12**) also provide insight into the different modeling approaches and the associated predicted behavior relative to experimental data. Except for submission 6, all predictions underpredicted the observed experimental behavior. The same relative behavior was not observed in the baseline cases, which consistently resulted in an overprediction of crack aspect ratio relative to the observed experimental behavior. What factors may be contributing to this discrepancy? As mentioned previously, recent investigations have indicated an initial shakedown of stresses resulting in redistribution of stress. In these investigations, the stresses near the bore of the hole are reduced (less compressive) and the overall stress field redistributes further away from the hole. This initial change in the residual stress field, which appears to stabilize at some point during cycling of the experimental coupons, may explain the discrepancy in both the predicted aspect ratios as well as the inability to predict the observed dip in the crack growth rate as shown in **figure 9**. It should be noted that the residual stresses utilized in the predictions were generated from experimental coupons that were not precycled; therefore, any initial redistribution of stress would not be captured in the input residual stress and the resulting analyses.

Conclusions

Overall, the round robin exercise proved to be quite beneficial, highlighting the differences in the approaches. For all cases, the predictions were consistent between similar analytical approaches, based on AFGROW, NASGRO, and FEA-FCG models, except for submission 6 for Cx holes, which tended to be an outlier relative to the other submissions. As a follow-on to the initial submissions, additional evaluations have been completed to dissect the predictions and understand the key contributing factors. This has born significant fruit, uncovering necessary improvements to analytical tools and methods, highlighting best practices, and identifying new focus areas moving forward. The results of these efforts will be documented in future releases of the analysis methods best practices document.[17]

ACKNOWLEDGMENTS

The authors would like to thank all those that participated in the round robin effort as well as the organizers and integrators of ERSI.

References

1. S. Carlson and R. T. Pilarczyk, "Using a Beta (β) Correction to Improve the Life Predictions of Cold-Expanded Holes in 2024-T3 & 7075-T6 Aluminum Alloys," *Materials Performance and Characterization* 7, no. 4 (2018): 779–806, https://doi.org/10.1520/MPC20170106
2. D. L. Andrew, P. N. Clark, and D. W. Hoeppner, "Investigation of Cold Expansion of Short Edge Margin Holes with Pre-existing Cracks in 2024-T351 Aluminum Alloy," *Fatigue & Fracture of Engineering Materials & Structures* 37, no. 4 (2014): 406–416, https://doi.org/10.1111/ffe.12123
3. S. S. Carlson, "Experimentally Derived Beta (β) Corrections to Accurately Model the Fatigue Crack Growth Behavior at Cold Expanded Holes in 2024-T351 Aluminum Alloys" (Master of Science thesis, University of Utah, 2008).
4. D. L. Andrew, "Investigation of Cold Expansion of Short Edge Margin Holes with Preexisting Cracks in 2024-T351 Aluminum Alloy" (Master of Science thesis, University of Utah, 2011).
5. M. B. Prime and A. T. DeWald, "The Contour Method," *Practical Residual Stress Measurement Methods*, ed. G. S. Schajer (West Sussex, UK: John Wiley & Sons, 2013), 109–138.
6. Fatigue Technology Inc., *FTI Tooling Catalog, Revision 7* (Seattle, WA: Fatigue Technology, Inc., 2014).
7. A. DeWald, M. Hill, J. VanDalen, B. Pilarczyk, D. Andrew, M. Thomsen, S. Carlson, and D. Marosok, "Residual Stresses from Cold Working of Aircraft Fastener Holes," in *Proceedings of the 2013 Aircraft Structural Integrity Program (ASIP) Conference* (Bonita Springs, FL: Universal Technology Company, 2013).
8. J. C. Newman Jr. and I. S. Raju, "Stress-Intensity Factor Equations for Cracks in Three-Dimensional Bodies Subjected to Tension and Bending Loads," in *Computational Methods in the Mechanics of Fracture*, ed. S. N. Atluri (Amsterdam, the Netherlands: Elsevier Science Publishers B.V., 1986), 311–334.
9. J. A. Harter, *AFGROW Users Guide and Technical Manual, AFRL-VA-WP-TR-1999-3016* (Wright-Patterson AFB, OH: Air Force Research Laboratory, 1999).

10. B. A. Szabó and I. Babuška, *Finite Element Analysis* (New York: John Wiley & Sons, Inc., 1991).
11. J. P. Pereira and C. A. Duarte, "The Contour Integral Method for Loaded Cracks," *Communications in Numerical Methods in Engineering* 22, no. 5 (2006): 421–432, https://doi.org/10.1002/cnm.824
12. *Standard Test Method for Measurement of Fatigue Crack Growth Rates* (Superseded), ASTM E647-00 (West Conshohocken, PA: ASTM International, approved December 10, 2000), https://doi.org/10.1520/E0647-00
13. S. S. Carlson, "Quantifying the Effect of a Fatigue Crack on the Residual Stress Field Induced by the Split Sleeve Cold Expansion Process in 2024-T351 and 7075-T651 Aluminum Alloys" (doctoral diss., University of Utah, 2018).
14. T. Mills, S. Prost-Domasky, and C. Brooks, "Fatigue Life Modeling at CX and Interference Holes" (paper presentation, A-10 ASIP Summit, Layto, UT, May 7–8, 2019).
15. M. D. Olson, A. T. DeWald, M. B. Prime, and M. R. Hill, "Estimation of Uncertainty for Contour Method Residual Stress Measurements," *Experimental Mechanics* 55 (2015): 577–585, https://doi.org/10.1007/s11340-014-9971-2
16. M. R. Hill and M. D. Olson, "Repeatability of the Contour Method for Residual Stress Measurement," *Experimental Mechanics* 54, no. 7 (2014): 1269–1277, https://doi.org/10.1007/s11340-014-9867-1
17. A-10 ASIP, *Analytical Considerations for Residual Stress Best Practices and Case Studies* (Fort Belvoir, VA: Defense Technical Information Center, 2018).